Design and Analysis of a W-Band Metasurface-Based Computational Imaging System

TOMAS ZVOLENSKY, JONAH N. GOLLUB, (Member, IEEE), DANIEL L. MARKS, AND DAVID R. SMITH, (Member, IEEE)

Department of Electrical and Computer Engineering, Center for Metamaterials and Integrated Plasmonics, Duke University, Durham, NC 27708 USA

Corresponding author: Tomas Zvolensky (permaloy@gmail.com)

ABSTRACT We design and numerically analyze a coherent computational imaging system that utilizes a sparse detector array of planar, frequency-diverse, metasurface antennas designed to operate over the W-band frequency range (75–110 GHz). Each of the metasurface antennas consists of a parallel plate waveguide, into which a center coaxial feed is inserted into the lower plate, launching a cylindrical guided wave. A dense array of metamaterial resonators patterned into the upper plate couples energy from the waveguide to free space radiative modes. The resonance frequency of each element, determined by its specific geometry, can be positioned anywhere within the W-band. The geometry of each element is chosen to produce a resonance frequency selected randomly from the W-band. Since a random subset of elements is resonant at any given frequency, the metasurface antenna forms a sequence of spatially diverse radiation patterns as a function of the excitation frequency. We analyze the metasurface aperture as an imaging system, optimizing key parameters relevant to image quality and resolution, including: aperture size; density and quality factor of the metamaterial resonators; number of detectors and their spatial distribution; bandwidth; and the number of frequency samples. A point-spread function analysis is used to compare the metasurface imager with traditional synthetic aperture radar. The singular value spectrum corresponding to the system transfer function and the mean-square-error associated with reconstructed images are both metrics used to characterize the system performance.

INDEX TERMS Computational imaging, metamaterials, metasurface, millimeter-waves, sparse antenna array.

I. INTRODUCTION

Microwave and millimeter waves have been routinely used for imaging in the medical, security, and aerospace fields [1]–[8], and have unique capabilities for certain applications such as composite material investigation or through-wall imaging. Specific imaging approaches such as synthetic aperture radar (SAR) [9] and phased arrays [10] are well-established but require long acquisition time, or costly feeding networks, respectively. Hybrid mechanical and electronic approaches, such as cylindrical scanners [11] and focal plane arrays [12] use SAR principles and achieve moderate acquisition times but do not provide an obvious roadmap to real-time imaging rates and compact system form factors. Principles of holographic imaging scheme used in this manuscript are described in detail in [13].

In recent work [13]–[15], an alternative imaging modality has been developed that combines computational imaging concepts with emerging metasurface architectures. The coherent, sparse imager analyzed in this paper leverages frequency diversity to achieve a large number of measurements, avoiding both mechanical scanning components as well as potentially expensive active components. The frequency-diverse metasurface imager thus trades expensive and elaborate hardware for increased data processing, relying on a fully determined model of the antenna radiation patterns and their scattering from targets in the scene, or the *forward model*.

There has been a steady stream of developments relating to the metasurface imager, culminating in compelling imaging demonstrations performed at frequencies in the K-band (18–26.5 GHz) [16], [17] using the planar waveguide approach. These experiments have proven the metasurface imager concept, and allowed key system parameters and features to be identified and optimized. In addition, a suite of computational tools has been created that enables

end-to-end modeling of the metasurface imager [18], which has been shown to predict imaging performance with excellent accuracy.

In this paper, we examine the possibility of scaling the metasurface imager to W-band frequencies (75-110 GHz), where potential capabilities such as increased resolution [19]– [21] and spectrum-based identification of dielectrics can be attractive advantages. While the underlying metasurface aperture concept scales trivially to shorter wavelengths in terms of the electromagnetics, a W-band imaging system presents particular challenges for image processing and reconstruction.

Consider a metasurface aperture designed for full-resolution imaging of human-sized targets. Such a system operating at K-band frequencies (18 – 26.5 GHz) was analyzed in [22]. For a 2 m × 2 m sized aperture, with resolution of 1.5 cm in range and 5 mm in cross-range, approximately 200,000 measurement modes, and 0.26 × 1 × 1.9 m region of interest dimensions, roughly 90 gigabytes of data is required for diffraction-limited resolution of the full scene (multiplying the number of modes, and voxels, assuming single precision).This is for the case of constrained region of interest (ROI) enveloping the target body decreasing the number of voxels from 872,336 to 122,000 [22].

A W-band system of the same size has diffraction-limited resolution on the order of 1 mm in cross-range at a center frequency of 92.5 GHz, and 4.3 mm resolution in range. The resulting number of diffraction limited scene voxels is proportionally larger at nearly 13 terabytes of data. Based on typical reconstruction approaches demonstrated to date and reasonably available computational power, full resolution images at W-band are thus not a practical goal—certainly not for fast, near real-time imaging.

A more realistic scenario for a W-band metasurface imager is one in which the target reconstruction volume is constrained, so that a vastly reduced number of measurements is required for diffraction-limited imaging. That is, rather than a human-scale target, just a small portion of the overall region would be imaged using the W-band aperture. To achieve high resolution over the constrained volume, a large aperture is still necessary, but the reduced number of measurements suggests that transmitting and receiving sub-apertures can sparsely populate the overall aperture. Such a W-band system could be, for example, co-integrated into a composite aperture for multiband operation, with a lower frequency aperture providing complete coverage of a target with lower resolution, while the W-band aperture can be used to provide high-resolution detail on certain smaller ROI.

Our goal here is to investigate the potential design of a sparse, metasurface aperture for W-band operation. We do not delve further into the system aspects, but note that to achieve a sparse imager implies that there is no reflection from any other objects in the scene outside of the particular ROI. In the envisaged operation, these objects would certainly reflect W-band radiation, and therefore some provision would be necessary to ensure the modes of the transmitting or receiving

aperture would have high gain. Such designs are possible, and represent a topic of future investigation [23]. Here, we concern ourselves with the image fidelity available from a sparse, W-band aperture, in which a small target is considered and no other objects are in the field-of-view. The reconstructed images thus represent a best-case scenario of what might be possible in an actual system.

In Section II, we present the basic W-band metasurface imager design and assess the expected resolution, considering such system parameters as: the number of transmitters; number of receivers; available SNR; spatial distribution of the antennas; antenna size; number of radiating elements and their quality factors; and Fourier (k-) space coverage.

In Section III, we outline those elements of the general computational imaging theory pertinent to our system. In Section IV, the imager parameters are determined through the PSF and trade-off studies based on EM simulation and Fourier coverage analysis [24].

II. METASURFACE IMAGER

The metasurface aperture consists of several frequency-diverse aperture antennas that each produce a sequence of complex radiation patterns whose spatial fields vary as a function of the excitation frequency. Each antenna consists of a parallel plate waveguide, the top conductor of which is patterned with an array of resonant metamaterial elements [25] (Fig. 1a). The resonance frequencies of the resonators are randomly selected across the W-band spectrum. While we do not detail the design of the metamaterial elements here, we note that we are assuming complementary electric resonators (cELCs), which scatter and radiate approximately as polarizable magnetic dipoles. The guided mode is modeled as a cylindrical wave excited at a known location on the antenna (in our case the geometrical center) to correctly calculate the phase of the exciting wave at each cELC. In the present context, we thus model the resonators as polarizable dipoles, simulating both the antennas and scattering from the scene using procedures previously reported [18].
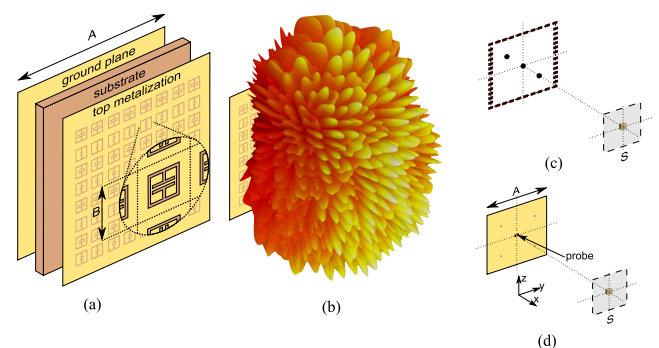

FIGURE 1. (a) An illustration of the metamaterial parallel plate antenna with characteristic cELC resonators etched into the top layer. (b) A plot of the radiation pattern of the metamaterial panels at a fixed frequency is shown. (c) The SAR imaging configuration used in the PSF analysis is shown, with a single voxel as a target in the region of interest S; (d) The modeled one panel and one probe frequency diverse imaging system is illustrated.

At any given excitation frequency, a subset of the metamaterial elements is excited; the elements off-resonance can be considered as "off," or non-transmissive. The corresponding field patterns feature a random pattern of lobes and nodes spread over a large angular region, as shown in Fig. 1b). Energy scattered by the target is detected by an array of low-gain, open-ended waveguide (OEWG) probes. By positioning the OEWG probes over a larger area, a sparse detector is formed, with the received power at each probe constituting a set of measurements (many frequency samples at each location).

Each measurement can be related to the scene reflectivity by the forward model. Since the smallest detectable volume is set by aperture and bandwidth limits, the scene can be discretized into a set of voxels, so that the finite set of measurements is related to the finite set of reflectivity values by

$$\bar{g} = \bar{H}\bar{f} + \bar{n}. \tag{1}$$

The dimension of the measurement vector, $\bar{g}$, is given by the total number of transmitters, receivers, and frequency points. Assuming the first Born approximation, the measurement matrix, $\bar{H}$, consists of elements of the form $H_{i,j} = E_{Tx,i}^j E_{Rx,i}^j$ [25]. Here, the subscript i indexes the transmit and receive antennas and the selected frequency sample; the superscript j refers to the jth voxel; $\bar{f}$ is the reflectivity of the target; $\bar{n}$ is a vector of random values that represents white Gaussian noise.

Due to the sparsity of the aperture and the random field patterns of the measurement modes, the system can, at best, approach the performance of a SAR imaging system. It should be noted that the number of voxels to be reconstructed is an arbitrary choice, so that the measurement matrix $\bar{H}$ will generally not be square. In fact, the expected resolution for a W-band system is on the order of the wavelength, meaning the number of voxels required for reconstruction of a human-sized target would vastly outnumber the number of measurement modes available. To achieve imaging with the sparse apertures considered here, we restrict the extent of the reconstruction region and consider relatively simpler targets.

With the system details incorporated into a measurement matrix, the image reconstruction process then consists of approximately inverting Eq. 1. We make use of two common reconstruction methods: matched filter and conjugate gradient. Matched filter does not require inversion of the $\bar{H}$ matrix, only a matrix multiplication step, or [26]

$$\bar{f}_e = \bar{H}^\dagger \bar{g}, \tag{2}$$

where $\bar{H}^\dagger$ is the Hermitian transpose of the measurement matrix $\bar{H}$. Since the measurement matrix is not necessarily square, the inverse cannot be defined exactly. The presence of noise and other real-world imperfections further obstruct direct inversion, which is why iterative methods such as conjugate gradient [27] are used at the expense of longer reconstruction time. These image estimation techniques take

the form of a minimization problem, or

$$\bar{f}_e = \arg\,min_{f_e} \left\| \bar{H}\bar{f}_e - \bar{g} \right\|_2^2. \tag{3}$$

Here, $arg\,min_{f_e}||\dots||$ is the least squares estimate of the f_e. Using suitable priors [28], [29], the number of measurements needed to recover the scene can be much smaller than the number of diffraction limited scene points, or voxels.

The resolution of a SAR system serves as a useful comparison with the sparse imager. SAR measurements are highly uncorrelated, being nearly orthogonal in Fourier space. The SAR resolution limit is $\delta_{CR} = \lambda R/(2D)$ for the cross range dimension and $\delta_R = c/(2BW)$ for the range dimension [30], where λ is the wavelength at the center frequency, R is the distance from the aperture to the target, D is the aperture size, c is the light velocity, and BW is the bandwidth. These limits can be used to roughly anticipate the number of modes needed to image a given target.

The W-band metasurface imaging system analyzed here is designed and simulated using a numerical tool previously reported [25]. A target is described as a collection of point scatterers with assigned reflectivity values; it is further assumed that the field inside the scattering volume is constant and equal to the impinging field—that is, multiple scattering events are not considered (Born approximation).

The point spread function (PSF) provides information on the transfer function of an imaging system and is thus a useful measure of overall performance. For reference, the PSF of a synthesized 100 mm × 100 mm aperture (Fig. 1c), with 100 frequency samples taken over the W-band, is shown in Fig. 2. For a single voxel target at a 1 m offset, the resulting PSF indicates resolution limits of 1.77 cm in cross range and 0.5 cm in range. The resolution of an equivalent size metasurface imager with one panel (with four feeding points) and one probe (see Fig. 1d) is 4.4 cm in cross range and 0.56 cm in range shown in Fig. 3 for matched filter reconstruction. For the least squares reconstruction method – described by equation (3) [31], the resolution in cross range is 2.5 cm and 0.5 cm in range (Fig. 4, for no noise conditions). Matched filter (MF), described by equation (2), does not require any constraints to be applied to the processed data effectively being the simplest and fastest reconstruction method with the image quality limited only by the number of available
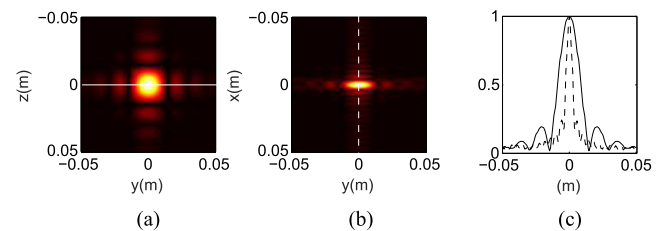

FIGURE 2. The point spread function of a SAR array with a size of 0.1 × 0.1 m consisting of 4400 transceiver probes, using matched filter reconstruction. 2D intensity images are shown for (a) cross range (*YZ* plane), (b) range (*XY* plane), and (c) 1D cuts for the case with no noise condition.
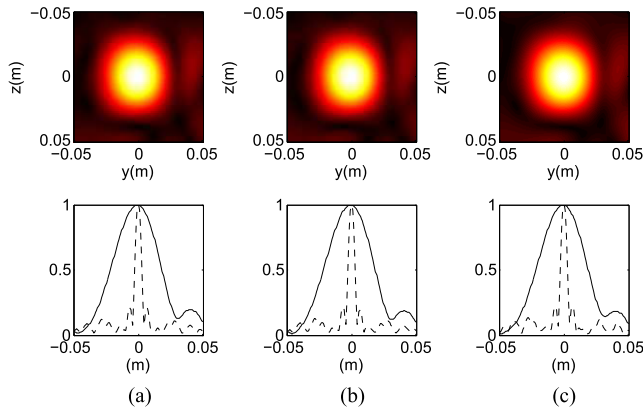
FIGURE 3. The 2D point spread function of a one panel, one probe, system using matched filter reconstruction is shown along with its associated intensity cuts in the range (dashed) and cross-range (solid) row for (a) no noise, (b) SNR = 15 dB, and (c) SNR = 5 dB.
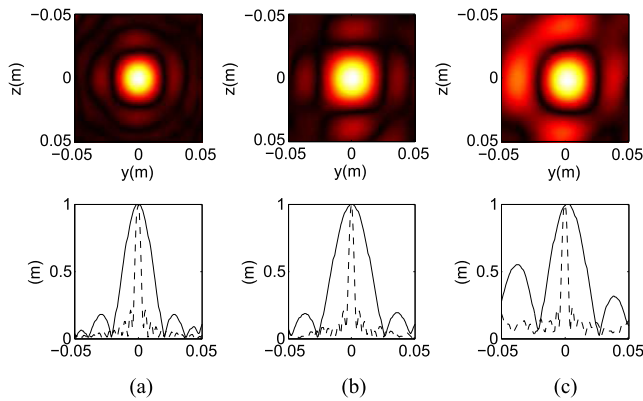

FIGURE 4. Point spread function of a one panel, one probe system using least squares reconstruction: 2D intensity images in top row, range (dashed) and cross range (full) cuts in bottom row for (a) no noise, (b) SNR = 15 dB, and (c) SNR = 5 dB.

measurement modes. Least squares (LS) on the other hand utilizes L2 norm optimization in order to improve the image quality compared to matched filter, but is as well time consuming due to the iterative nature of the process.

In the limiting case of the number of measurements being equal to the number of diffraction limited voxels, MF image would correspond to SAR quality (making it robust towards noise). Because we utilize a very small number of measurements, the PSF image shows signs of deterioration, which can be compensated using LS but with increased sensitivity to noise conditions. LS reconstruction is equivalent to inverse of singular values, so in case of low SNR the noise is amplified, which can be avoided using additional regularization techniques [22].

III. SYSTEM TRADE-OFF STUDIES

The benefits of the metasurface imager come at the cost of increased design complexity, greater required knowledge of the forward model, and increased processing power. Using the numerical simulations is therefore vital in identifying the

key parameters of the frequency diverse panels and overall system relevant to image quality. The simulated imaging capability of a 1 m sized aperture consisting of multiple panels and probes (Fig. 5a) is considered in Fig. 5b). The aperture consists of 16 panels, each with a dimension of 10 cm and a 1 mm pitch size, resulting in ten thousand elements per panel, 12 randomly distributed probes are used as receive antennas. The use of low-gain probes eases potential alignment sensitivities that would arise if one were to use the panels for both transmit and receive. As a first operational example, a 3 mm resolution target is reconstructed using both the matched filter (Fig. 5b top) and least squares (Fig. 5b bottom) methods. A number of design parameters can be varied to optimize the performance of the system, including the overall number of panels N_{pa}; the number of probes N_{pr}; the spatial distribution of panels and probes; the number of frequency points N_f; the overall bandwidth BW; the size B of the metamaterial resonator cell (see Fig. 1a); the quality factor of the elements Q_{elem}; and, the size of the transmitting antennas A.
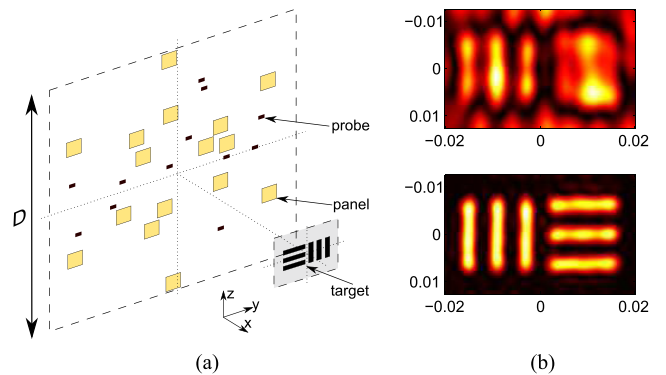

FIGURE 5. (a) An illustration of the full aperture (with size D) with an array of panels shown in Fig. 1(b) and probes of open-ended waveguides (black rectangles). (b) The simulation results of a reconstructed 3 mm resolution target using matched filter (upper) and least squares (lower) methods is shown.

Since the search space for each of the mentioned parameters is broad, a set of parametric studies is useful and necessary to tailor the system design to operate in the W-band. On top of the initial design, interdependency of the parameters indicates the challenges of achieving optimization through purely analytic means.

Guided by prior results for lower frequency metasurface aperture systems [19]–[21], the initial parameters are chosen as follows: $A = 10$ cm, $B = 0.1$ cm, $Q_{elem} = 100$, $N_f = 100$. The choice of operation bandwidth $BW = 75 - 110$ GHz is motivated with an eventual goal of increased spatial resolution and detection of dielectrics. The size of the aperture, $D = 1$ m is chosen, to achieve resolution on the order of millimeters. The critical metrics used for the evaluation of system performance are the singular value spectrum and the

mean-square error (MSE) given as

$$MSE = \frac{1}{\sum\limits_{n=1}^{N} \left| f_{R_n} \right|^2} \sum_{n=1}^{N} \left| f_{est_n} - f_{R_n} \right|^2 \quad (4)$$

Where f_{est} is the scene estimate based on the simulation and f_R is the known scene reference. A standard resolution target with bar width of 3 mm (scene size $S = 30 \times 50$ mm) (Fig. 5) is used throughout as the evaluation target.

A comparison of the full aperture resolution to the SAR limits for the two reconstruction methods is summarized in Table I. As in the case of the PSF described above, with the iterative reconstruction method, the resolution of the sparse system approaches SAR performance.

TABLE 1. Resolution of 1m sparse metasurface aperture compard to SAR limit using matched filter (MF) and least squares (LS) reconstruction methods.

		δ_R(mm)	δ_{CR} (mm)
SAR		4.2	1.6
Meta	MF	5.4	2.8
surface	LS	4.4	2.0

Calculating the singular value decomposition (SVD) of the measurement matrix H provides information regarding the orthogonality of the measurements. For the SAR example, there is minimal redundant information among the measurements (any correlation introduced arises from finite aperture effects); the singular value spectrum is thus nearly flat as a function of mode number, decaying slowly (Fig. 6a). By comparison, the singular value spectrum for the metasurface aperture decays rapidly with mode number, and cuts off early since the total number of measurements is limited in the sparse aperture. The available information content for the sparse aperture is thus significantly reduced. A scene occupying the full field-of-view of the metasurface aperture configured as in Fig. 5(a) could therefore not be reconstructed; however, by reducing the scene extent, fewer modes are required and the available measurements can provide useful images (and at high resolution). To illustrate this point, in Fig. 6(b), the singular value spectrums of the SAR and metasurface apertures are presented for a planar reconstruction surface, a distance of 1 m from the aperture and parallel to the plane of the aperture, and having dimensions of 100 mm × 100 mm. Compared to 1 m × 1 m ROI, the SVD spectrums are closer to each other indicating that the systems can have qualitatively similar performance.

The number of measurements can be adjusted by adding or removing metasurface panels. To investigate the impact of additional panels, we increase the number of panels N_{pa} while keeping all other parameters fixed. Singular value spectrums are displayed in Fig. 7a) for $N_{pa} = 4, 16, 25 \ldots 49$. A similar analysis is also performed for the number of receiving probes N_{pr} (regular distribution of both panels and probes), using 16 transmitting panels (Fig. 7b). Based on this
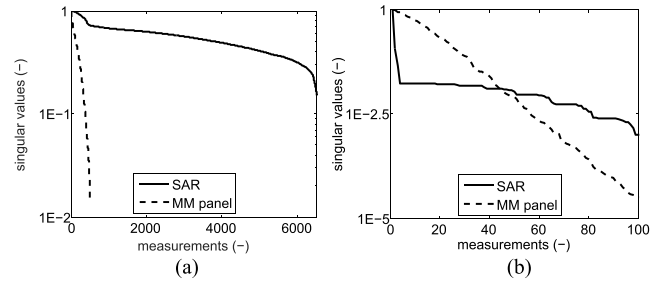

FIGURE 6. Singular values spectra of SAR simulated system and equivalent frequency diverse metamaterial system for (a) 1 × 1 m region of interest (ROI), and (b) 0.1 × 0.1 m ROI.
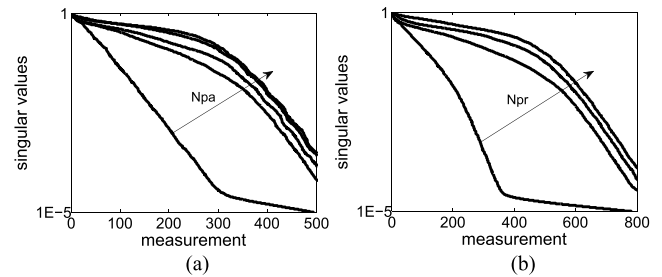

FIGURE 7. The normalized SVD spectra of (a) N_{pa} and (b) N_{pr} sweep (arrows point in direction of increasing number of elements in the arrays with the lines corresponding to 4, 16, 25, 36, and 49 antennas). A saturation point can be observed for approximately $N_{pa} = 16$ and $N_{pr} = 12$.
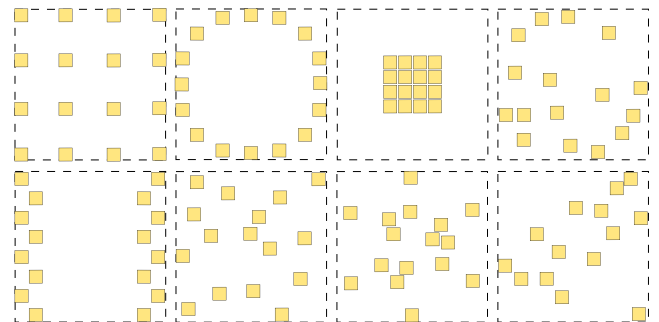

FIGURE 8. Spatial distributions of the panels tested, top row: regular, circular, full, maximal phase centers; and, bottom row: pillar, random, Golay, and fractal.

analysis, increasing the N_{pa} above 16 and N_{pr} above 12 does not improve the information content of the underlying modes significantly, since the space-bandwidth product (SBP) is reached for the constrained reconstruction region. Thus the number of panels and probes is fixed for the following studies.

With the aperture size maintained constant, the spatial distribution of the antennas and detectors has a significant influence on the singular value spectrums that characterize the measurement matrix, as well as the MSE values obtained from image reconstructions. In Fig. 8 and Fig. 9, spatial distributions of the panels, and the corresponding singular value spectrums and MSE values are shown, revealing that the "maximal" layout pattern represents an adequate balance between information content and reconstruction error. Fourier (k-) space coverage [32] provides an additional indicator as to the number of spatial frequencies covered by
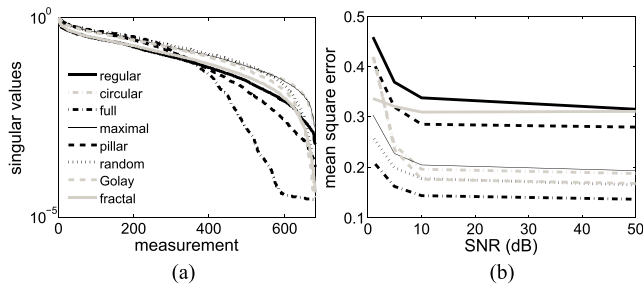
FIGURE 9. (a) The SVD spectra and (b) The MSE values for the various spatial distribution schemes of the antennas. MSE values are plotted against the SNR to estimate the acceptable noise levels.
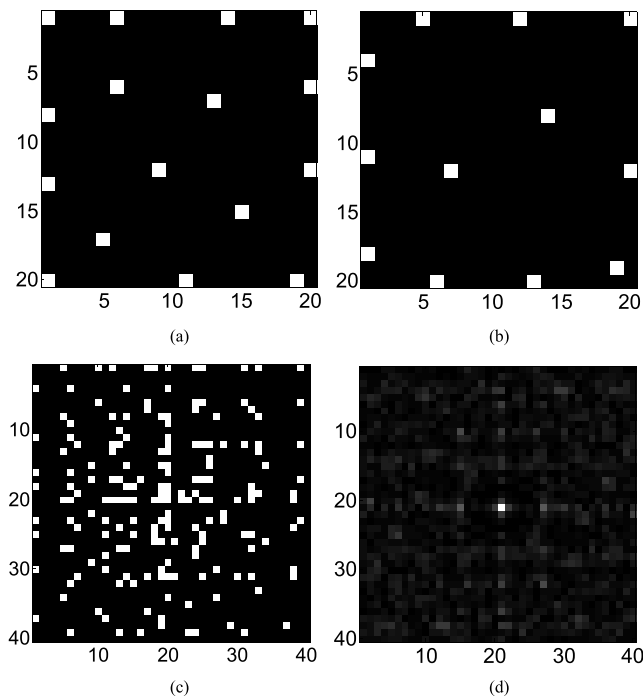

FIGURE 10. (a) The spatial distribution of the transmitting panels S_{Tx}; (b) the receiving probes S_{Rx}; (c) the k-space coverage of the Tx and Rx arrays obtained by convolution of the spatial distributions–$S^*_{Tx}S_{Rx}$; and, (d) PSF of the system.

FIGURE 11. Two dimensional maps of MSE dependence on the (a) *B* vs. N_f, (b) Q_{elem} vs. N_f, (c) Q_{elem} vs. *BW*, (d) *B* vs. *A*. The SNR chosen for this study is 10 dB in order to approximate expected noise level of a real imaging system.

the available measurement modes. In Fig. 10 an example of the k-space coverage is shown for one of the investigated spatial layouts. Comparing the considered cases, the maximal distribution provides the best coverage and smallest side-lobe level of the PSF and is used for the following trade off studies. The presence of the aliasing in the PSF is caused by sparse spatial sampling of the scene and is a natural and unavoidable occurrence with under-sampled imaging systems but can be mitigated using advanced reconstruction algorithms as shown in [22].

In Fig. 11, the MSE dependence on various system parameters is shown (using a 3 mm resolution target), indicating a quasi-linear dependence on N_f (Fig. 11a). If more than 40 frequency points are used, the reconstruction error has little dependence on the quality factor Q_{elem} (Fig. 11b).
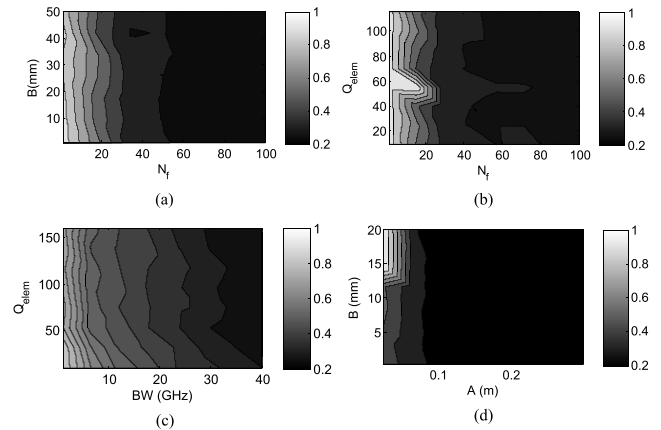
This implies we have fully spatially sampled the aperture [33]. This is fortunate, given the technological difficulty of obtaining high quality resonators (due to material losses) at W-band frequencies using printed circuit technology [34], unless special materials are used. However, these special materials are inherently costly and thus not compatible with economical systems. Due to the relative independence of the MSE on the quality factor of the radiating elements, for practically feasible system design, non-resonant or weakly-resonant elements are considered for future iterations of the whole system.

Figure 11(c) further confirms the relative independence of the system performance on Q_{elem} and reveals a linear dependence on the bandwidth *BW*. With regard to the remaining simulations, we choose 100 frequency points and a 35 GHz bandwidth, since the W-band extension heads commercially available commonly have such bandwidth available. Fig. 11d) suggests the element pitch *B* for this aperture should be kept below 12 mm. The optimal size of *A* spans between 0.1 and 0.2 m, where the upper boundary is given with regard to physical implementation of a small aperture (D = 1m) and increasing alignment issues. The parameters obtained here are application specific and do not serve as an exhaustive analysis, since the performance of an imaging system is a function of many degrees of freedom. Nevertheless, this analysis can be taken as a guideline for similar systems while being attentive to the specific requirements.

IV. CONCLUSIONS

A W-band compressed imaging system leveraging the computational imaging techniques was designed. A point spread function analysis proved the advantage of the frequency diverse imager over traditional SAR, significantly decreasing the acquisition time while the image quality remained comparable when using iterative reconstruction methods.

Minimum viable system requirements were determined for a full sized 1 m × 1 m aperture using the singular

value spectrum of the measurement modes; the MSE – a comparison of reference and resolved image; and, k-space coverage. The optimized parameters were found as follows: 16 transceiver antennas, 12 receiving probes with random distribution, $Q_{elem} \leq 100$, $A = 10$ cm, $B \leq 5$ mm, $D = 1$ m, $SNR = 10$ dB, $N_f = 100$. Although the achievable quality factor of the metamaterial elements in the W-band frequency regime is low (resulting in unavoidable correlation of the measurement modes), through optimization of the full system parameters, a viable imaging system was designed. At W-band frequencies the motivation for harnessing computational methods becomes extremely compelling compared to the K-band systems, where moderate quality factor values are still technologically feasible.

Demonstrations of random mode imaging of human size targets at lower frequencies (K-band) rely heavily on the computational power. Scaling the discretization mesh to W-band frequencies renders this imaging scheme computationally prohibitive. Substantially higher path loss (resulting into lower SNR of the measured data) adds further challenges in using broadly radiating random mode panels. A "spotlight" imaging scheme, however, can elegantly address both issues, collimating power only on the 'zoom-in' high-resolution area of the target (e.g. threat detection on the human body). The spotlight approach will ultimately require rough beam forming capabilities. Approaches such as [23], [35] have proven that low cost systems at K-band are viable, and suggest that similar systems could befeasible at W-band.

ACKNOWLEDGMENT

REFERENCES

[1] J. T. Case, S. Kharkovsky, R. Zoughi, G. Steffes, and F. L. Hepburn, "Millimeter wave holographical inspection of honeycomb composites," in *Proc. AIP Conf.*, Melville, NY, USA, 2008, pp. 970–975.

[2] S. Hantscher, A. Reisenzahn, and C. G. Diskus, "Through-wall imaging with a 3-D UWB SAR algorithm," *IEEE Signal Process. Lett.*, vol. 15, pp. 269–272, Feb. 2008.

[3] R. Zoughi, "Material characterization," in *Microwave Non-Destructive Testing and Evaluation*. The Netherlands: Kluwer.

[4] N. K. Nikolova, "Microwave imaging for breast cancer," *IEEE Microw. Mag.*, vol. 12, no. 7, pp. 78–94, Dec. 2011.

[5] L. E. Larsen and J. H. Jacobi, "Introduction," in *Medical Applications of Microwave Imaging*. New York, NY, USA: IEEE Press.

[6] D. M. Sheen, D. L. McMakin, and T. E. Hall, "Three-dimensional millimeter-wave imaging for concealed weapon detection," *IEEE Trans. Microw. Theory Techn.*, vol. 49, no. 9, pp. 1581–1592, Sep. 2001.

[7] J. T. Case, S. Kharkovsky, R. Zoughi, and F. Hepburn, "High resolution millimeter wave inspecting of the orbiter acreage heat tiles of the space shuttle," in *Proc. IMTC*, Warsaw, Poland, 2007, pp. 1–4.

[8] C. Huber, H. Abiri, S. I. Ganchev, and R. Zoughi, "Modeling of surface hairline-crack detection in metals under coatings using an open-ended rectangular waveguide," *IEEE Trans. Microw. Theory Techn.*, vol. 45, no. 11, pp. 2049–2057, Nov. 1997.

[9] C. W. Sherwin, J. P. Ruina, and R. D. Rawcliffe, "Some early developments in synthetic aperture radar systems," *IRE Trans. Military Electron.*, vol. 6, no. 2, pp. 111–115, Apr. 1962.

[10] B. deB Frederick, L. L. Wald, L. C. Maas, and P. F. Renshaw, "A phased array echoplanar imaging system for fMRI," *Magn. Reson. Imag.*, vol. 17, no. 1, pp. 121–129, 1999.

[11] D. M. Sheen, D. L. McMakin, T. E. Hall, and R. H. Severtsen, "Active millimeter-wave standoff and portal imaging techniques for personnel screening," in *Proc. IEEE HST Conf.*, Waltham, MA, USA, May 2009, pp. 440–447.

[12] P. F. Goldsmith, C.-T. Hsieh, G. R. Huguenin, J. Kapitzky, and E. L. Moore, "Focal plane imaging systems for millimeter wavelengths," *IEEE Trans. Microw. Theory Techn.*, vol. 41, no. 10, pp. 1664–1675, Oct. 1993.

[13] J. Hunt *et al.*, "Metamaterial apertures for computational imaging," *Science*, vol. 339, pp. 310–313, Jan. 2013.

[14] G. Lipworth *et al.*, "Metamaterial apertures for coherent computational imaging on the physical layer," *J. Opt. Soc. Amer. A, Opt. Image Sci.*, vol. 30, no. 8, pp. 1603–1612, 2013.

[15] J. Hunt *et al.*, "Metamaterial microwave holographic imaging system," *J. Opt. Soc. Amer. A, Opt. Image Sci.*, vol. 31, no. 10, pp. 2109–2119, 2014.

[16] O. Yurduseven, V. R. Gowda, J. N. Gollub, and D. R. Smith, "Printed aperiodic cavity for computational and microwave imaging," *IEEE Microw. Wireless Compon. Lett.*, vol. 26, no. 5, pp. 367–369, May 2016.

[17] O. Yurduseven, J. N. Gollub, D. L. Marks, and D. R. Smith, "Frequency-diverse microwave imaging using planar Mills-Cross cavity apertures," *Opt. Exp.*, vol. 24, no. 8, pp. 8907–8925, Apr. 2016.

[18] G. Lipworth *et al.*, "Comprehensive simulation platform for a metamaterial imaging system," *Appl. Opt.*, vol. 54, no. 31, pp. 9343–9353, 2015.

[19] M. F. Fetterman, J. Grata, G. Jubic, W. L. Kiser, Jr., and A. Visnansky, "Simulation, acquisition and analysis of passive millimeter-wave images in remote sensing applications," *Opt. Exp.*, vol. 16, no. 25, pp. 20503–20515, Dec. 2008.

[20] D. A. Wikner and G. Samples, "Polarimetric passive millimeter-wave sensing," *Proc. SPIE*, vol. 4373, pp. 86–93, Aug. 2001.

[21] S. E. Clark, J. A. Lovberg, C. A. Martin, and V. G. Kolinko, "Passive millimeter-wave imaging for airborne and security applications," *Proc. SPIE*, vol. 5077, pp. 16–21, Aug. 2003.

[22] O. Yurduseven, J. N. Gollub, A. Rose, D. L. Marks, and D. R. Smith, "Design and simulation of a frequency-diverse aperture for imaging of human-scale targets," *IEEE Access*, vol. 4, pp. 5436–5451, Aug. 2016.

[23] T. Sleasman, M. F. Imani, J. N. Gollub, and D. R. Smith, "Dynamic metamaterial aperture for microwave imaging," *Appl. Phys. Lett.*, vol. 107, no. 20, p. 204104, 2015.

[24] D. J. Brady, K. Choi, D. L. Marks, R. Horisaki, and S. Lim, "Compressive holography," *Opt. Exp.*, vol. 17, no. 15, pp. 13040–13049, Jul. 2009.

[25] J. Hunt, "Metamaterials for computational imaging," Ph.D. dissertation, Dept. Elect. Comput. Eng., Duke Univ., Durham, NC, USA, 2013.

[26] S. M. Kay, *Fundamentals of Statistical Signal Processing: Detection Theory* (Prentice-Hall Signal Processing Series), vol. 2. Englewood Cliffs, NJ, USA: Prentice-Hall, 1998.

[27] R. Barrett *et al.*, *Templates for the Solution of Linear Systems: Building Blocks for Iterative Methods*, 1st ed. Philadelphia, PA, USA: SIAM, 1987, pp. 12–31.

[28] Y. Liu, L. Tian, J. W. Lee, H. Y. Huang, M. S. Triantafyllou, and G. Barbastathis, "Scanning-free compressive holography for object localization with subpixel accuracy," *Opt. Lett.*, vol. 37, no. 16, pp. 3357–3359, Aug. 2012.

[29] C. F. Cull, D. A. Winker, J. N. Mait, M. Mattheiss, and D. J. Brady, "Millimeter-wave compressive holography," *Appl. Opt.*, vol. 49, no. 19, pp. E67–E82, 2010.

[30] R. Sullivan, *Radar Handbook*, M. Skolnik, Ed., 3rd ed. New York, NY, USA: McGraw-Hill, 2008, ch. 17.

[31] O. Yurduseven *et al.*, "Resolution of the frequency diverse metamaterial aperture imager," *Prog. Electromagn. Res.*, vol. 150, pp. 97–107, Jan. 2015.

[32] A. P. Dhawan, *Medical Image Analysis*, 1st ed. Hoboken, NJ, USA: IEEE Press, 2003, pp. 27–29, 37–39, 62–91, 111–174, 62–91, and 111–174.

[33] D. L. Marks, J. Gollub, and D. R. Smith, "Spatially resolving antenna arrays using frequency diversity," *J. Opt. Soc. Amer. A, Opt. Image Sci.*, vol. 33, no. 5, pp. 899–912, 2016.

[34] V. N. Nguyen, "Design, analysis, and characterization of metamaterial quasi-optical components for millimeter-wave automotive radar," Ph.D. dissertation, Duke Univ., Durham, NC, USA, 2013.

[35] T. Sleasman, M. Boyarsky, M. F. Imani, J. N. Gollub, and D. R. Smith, "Design considerations for a dynamic metamaterial aperture for computational imaging at microwave frequencies," *J. Opt. Soc. Amer. B, Opt. Phys.*, vol. 33, no. 6, pp. 1098–1111, 2016.

TOMAS ZVOLENSKY received the M.Sc. degree in radio science and engineering from the Brno University of Technology, Brno, Czech Republic, in 2008, and the Ph.D. degree in radio science and engineering from Aalto University, Espoo, Finland, in 2014. Since 2016, he has been with a startup company Teraphic, a part of research and development and business development commercializing 3-D printing technologies for millimeter-wave applications. His main research interests include metamaterials, leaky-wave antennas, composite right/left-handed structures, tunable millimeter-wave antennas and devices, development of imaging capabilities of meta-surfaces in millimeter-wave range, and targeting security imaging applications.

JONAH N. GOLLUB (M'16) received the B.A. degree in physics from Reed College in 2000 and the Ph.D. degree in physics from the University of California at San Diego, San Diego, in 2009. His thesis was on characterizing the hybridization of metamaterials with magnetic materials. From 2010 to 2012, he was a Lead Modeling and Simulation Scientist with a startup company, where he was involved in developing surface meta-materials with applications targeted toward imaging and biological detection under DARPA, MDA, Army, and NSF funded efforts. He joined Duke University as a Research Scientist in 2013, where he is currently focused on developing real-time millimeter wave imaging approaches, which utilize frequency diverse antennas and compressive imaging techniques.

DANIEL L. MARKS was born in Chicago, IL, USA, in 1973. He received the B.S., M.S., and Ph.D. degrees from the University of Illinois at Urbana–Champaign, in 1995, 1998, and 2001, respectively. From 2001 to 2008, he was a Research Scientist with the Biophotonics Laboratory, University of Illinois at Urbana–Champaign. He has been an Associate Research Professor with the Department of Electrical and Computer Engineering, Duke University, since 2009. He has authored 85 research articles and holds 17 patents. His research interests include optics, optical design, computational imaging, millimeter-wave and terahertz imaging, metamaterials, and synthetic electromagnetic structures. He has been an Editor of the *Applied Optics*.

DAVID R. SMITH (M'98) received the Ph.D. degree in physics from the University of California at San Diego (UCSD), in 1994. He is currently the Department Chair and the James B. Duke Professor of Electrical and Computer Engineering with Duke University and the Director of the Center for Metamaterials and Integrated Plasmonics. He is also an Adjunct Professor with the Physics Department, UCSD, an Affiliate Faculty Member with the Electrical and Computer Engineering Department, University of Washington, and a Visiting Professor of Physics with the Imperial College London, London. His research interests include the theory, simulation, and characterization of unique electromagnetic structures, including photonic crystals and metamaterials, and the applications of such materials.

He and his colleagues demonstrated the first left-handed (or negative index) metamaterial at microwave frequencies in 2000 while at UCSD. He has authored over 200 publications on matematerials and plasmonics. In 2002, he was elected as a member of the Electromagnetics Academy. In 2005, he was part of a five-member team that received the Descartes Research Prize by the European Union for their contributions to metamaterials and other novel electromagnetic materials. He received the Stansell Research Award from the Pratt School of Engineering, Duke University, in 2005. In 2006, he was selected as one of the Scientific American 50, a group recognized by the editors of Scientific American for achievements in science, technology, and policy. His work has appeared twice on the cover of Physics Today, and twice has been selected as one of the Top Ten Breakthroughs of the year by the Science Magazine. In 2013, he was a co-recipient of the James C. McGroddy Prize for New Materials by the American Physical Society. He was selected by the ISI-Reuters as a Citation Laureate in 2009 for the most number of highly cited papers in physics over the last decade. He was once again recognized as one of the Highly Cited Researches 2014 by ISI-Reuters in the category of physics.

In 2006, he along with his colleague Prof. J. Pendry, suggested metamaterials could be used to design an electromagnetic cloak, introducing the new design tool of transformation optics. In 2013, he was asked to write an op-ed piece for the New York Times on cloaking research.

He served as the Founding and the Acting Director of the Metamaterials Commercialization Center, a unit within the Intellectual Ventures, Bellevue, WA, USA, in 2013, dedicated to commercializing metamaterials concepts. MCC has thus far produced three spin out companies: Kymeta Corporation, Redmond, WA, Evolv Technologies, Waltham, MA, USA, and Echodyne, Bellevue. He is a Co-Founder of Evolv Technologies, which targets metamaterial apertures for security screening applications, and Echodyne, which is seeking to apply metamaterial apertures to radar applications. He serves on the Advisory Board for Kymeta, which targets metamaterial-based antennas for satellite communications.

● ● ●